BEAM DYNAMICS STUDY CONCERNING SIS-100 PROTON OPERATION INCLUDING SPACE CHARGE EFFECTS

S. Sorge*, GSI, Darmstadt, Germany

Abstract

The projected SIS-100 synchrotron at GSI will be used for operation with intense proton and heavy ion beams. In order to avoid the crossing of the transition energy during proton operation a complicated optics scheme is proposed to provide a transition energy above the extraction energy of $E = 29$ GeV. For the purpose of optimizing the lattice, and to find a suitable working point, regime simulation scans of the dynamic aperture are performed based on MAD-X tracking. In the next step working point candidates will be used for particle tracking simulations in order to estimate beam loss due to space charge induced resonance crossing. For these studies different codes and space charge models are considered.

LATTICE PROPERTIES

Besides heavy ion operation, the SIS-100 synchrotron is also foreseen to deliver high intensity proton beams of 2.0×10^{13} protons in a short single bunch. The particles will be injected at $E_{in} = 4$ GeV and fast extracted at $E_{ex} = 29$ GeV. The working point is still under discussion. In this study, $(Q_x, Q_y) = (21.8, 17.7)$ is used.

In order to stay below transition energy, linear optics were developed that provide a transition energy corresponding to $\gamma_{tr} = 45.5$. Applying three independent families of quadrupoles, the strongly oscillating dispersion function represented by the red curve in Fig. 1 will be created. In doing so the momentum compaction factor

$$\alpha_c = \frac{1}{\gamma_{tr}^2} = \frac{1}{C} \oint \frac{D_x(s)\mathrm{d}s}{\rho(s)} \qquad (1)$$

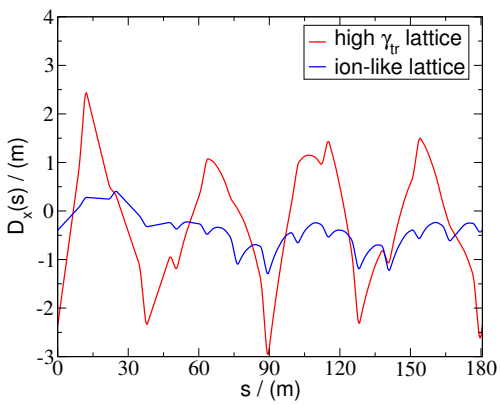

Figure 1: Dispersion function of the high γ_{tr} lattice in one of six SIS-100 sectors compared to that of an "ion-like" lattice of the same working point.

* S.Sorge@gsi.de

Table 1: Maximum values of some lattice functions of high γ_{tr} lattice and ion-like lattice, both at the working point is $(21.8, 17.7)$. 2σ emittances are $(\epsilon_{x,2\sigma}, \epsilon_{y,2\sigma}) = (13 \times 4)$ mm mrad are assumed. The natural chromaticities in row 6 correspond to Eq. (2).

	high γ_{tr}	ion-like
quadrupole families	3	2
γ_{tr}	45.5	18.4
$D_{x,max}/(\mathrm{m})$	2.9	1.3
$(\beta_{x,max}, \beta_{y,max})/(\mathrm{m})$	$(72, 29)$	$(19, 21)$
max. 2σ beam widths at $\delta = 0$, (h,v)/(mm)	$(31, 11)$	$(16, 9)$
$(\xi_{x,nat}, \xi_{y,nat})$	$(-2.4, -1.4)$	$(-0.9, -1.1)$

is minimised. The extrema of the high γ_{tr} dispersion function are much higher than those of the dispersion function generated with two quadrupole families used during heavy ion operation. In addition, the usage of the high γ_{tr} quadrupole settings increases other lattice variables, see Table 1. The chromaticities $\xi_{x,nat}, \xi_{y,nat}$ shown in that table are defined by

$$\Delta Q = \delta \xi Q. \qquad (2)$$

MAGNET IMPERFECTIONS AND RESONANCES

Real magnets are with imperfections. In particular random gradient errors in the main quadrupoles lead to an increase of the maximum horizontal beta function. Assuming them to follow a Gaussian distribution truncated at 2σ with the relative rms width of $\sigma_{rel} \approx 0.003$ of the averaged focusing strength of all quadrupole families, the maximum horizontal beta function becomes increased from 72 m to about 100 m, the exact value depends on the actual sample of random errors. In addition, there are non-linear multipole errors in main dipoles and quadrupoles each consisting of a systematic and a random contribution. The systematic components depend on $B\rho$ [1]. The random components are assumed to follow a Gaussian distribution truncated at 2σ with σ be 30 % of the corresponding systematic component. In particular the random components drive non-linear resonances which restrict the choice of the working point. To make them visible and to find a suitable working point, the dynamic aperture was determined at 100×100 working points in the range $Q_x \in [21, 22], Q_y \in [17, 18]$. The result is shown in Fig. 2. For $Q_x < 21.5$ dynamic apertures could not be determined because the lattice properties are too difficult for MAD-X even to determine the lattice functions

ISBN 978-3-95450-116-8

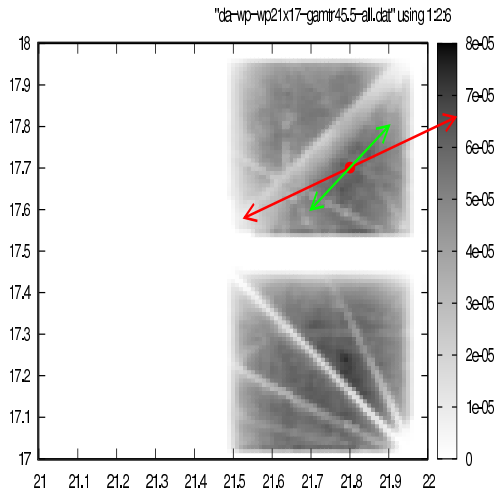

Figure 2: Resonance diagram, working point and tune spread due to $\delta = \pm 0.005$ and chromaticity without (red curve) and with (green curve) correction obtained for $\gamma_{tr} = 45.5$.

there. That is a severe restriction to the working point. So, the tune scan confirms the working point mentioned above.

The large natural chromaticities and the maximum momentum spread of $\delta_m = \pm 0.005$, reached at $E = 7$ GeV where the rf voltage reaches its maximum value, create the chromatic tune spread $(\Delta Q_x = \pm 0.27, \Delta Q_y = \pm 0.12)$, see the red arrow in Fig. 2. Because the tune spread does not fit between the half integer resonance at $Q_x = 21.5$ and the integer resonance at $Q_x = 22$ it needs to be reduced. Otherwise, particles with large δ will become lost within a synchrotron period.

CHROMATIC TUNE SPREAD AND DYNAMIC APERTURE

The reduction of the tune spread was done in two steps.

The first step consists in correcting the chromaticity with all 52 sextupoles in SIS-100 in order to achieve $\Delta Q_{x,max} = \Delta Q_{y,max} = \pm 0.1$ to make the chromatic tune spread fit in the mesh of resonances, see the green arrow in Fig. 2. The usage of 52 sextupoles to correct two variables, ξ_x, ξ_y, allowed to set the additional constraint to their focusing strengths $k_2 L$

$$\sum_{n=1}^{52} (k_2 L)_n^2 \rightarrow \text{minimum} \qquad (3)$$

in order to avoid strong sextupoles.

The second step consists in using the high-γ_{tr} settings only at high energies. At low energies the ion-like lattice described in the right column of Table 1 is applied as long as $\gamma_{tr}(E) < 18.4$, where $\gamma_{tr}(E)$ is determined by

$$\eta(E) = \frac{1}{\gamma^2} - \frac{1}{\gamma_{tr}^2(E)} = \text{const.} \qquad (4)$$

with $\gamma_{tr}(E = 29 \text{ GeV}) = 45.5$. The simplest indicator that shows the advantage of that way to proceed is the so

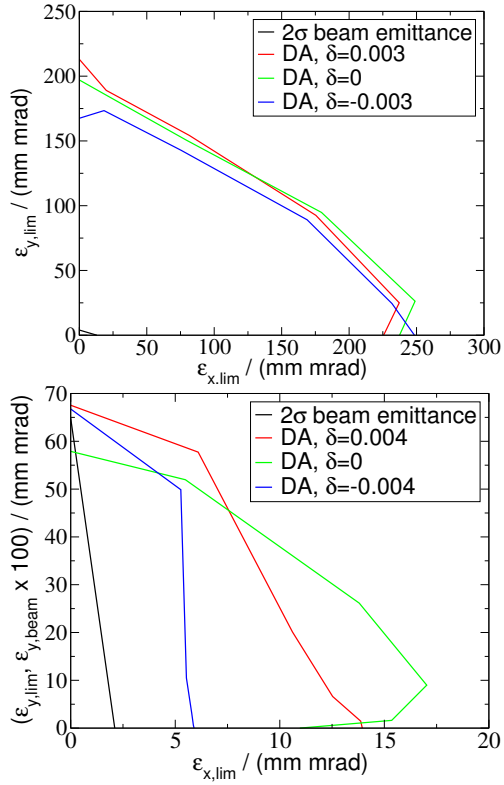

Figure 3: Dynamic apertures calculated with ion-like optics at $E = 4$ GeV (graph above) and high-γ_{tr} optics for $E = 29$ GeV (graph below). Both graphs contain curves for $\delta = 0, \pm\delta_m$ where $\delta_m = 0.003$ at 4 GeV and $\delta_m = 0.004$ at 29 GeV. The 2σ beam emittances are (13×4) mm mrad and (2.1×0.7) mm mrad, respectively. In the graph below, the vertical beam emittance is multiplied by 10.

called diagonal dynamic aperture

$$\epsilon_{lim,x}(\phi) = \epsilon_{lim}(\phi) \cos^2 \phi, \ \epsilon_{lim,y}(\phi) = \epsilon_{lim}(\phi) \sin^2 \phi \qquad (5)$$

with the angles $\phi = (0, 0.1 \cdot \pi, 0.2 \cdot \pi, 0.3 \cdot \pi, 0.4 \cdot \pi, 0.5 \cdot \pi)$. $\epsilon_{lim}(\phi)$ was determined by means of single particle tracking for $\delta = 0, \pm\delta_m$ over a period of 500 turns. Figure 3 shows the dynamic apertures for $E = 4$ GeV, $\gamma_{tr} = 18.4$, and for $E = 29$ GeV, $\gamma_{tr} = 45.5$. At 4 GeV the dynamic aperture is much larger than the 2σ beam emittance, whereas at 29 GeV and for $\delta = -0.004$, the horizontal dynamic aperture is smaller than four times the horizontal beam emittance. In other words, the spatial horizontal dynamic aperture is smaller than twice the horizontal beam width.

MULTI-PARTICLE SIMULATION

The important quantity is the number of lost particles. To estimate it, multi-particle tracking simulations were performed using the thin-lens tracking tool of MAD-X. The used lattice contained an rf cavity in order to introduce synchrotron oscillations.

At the present stage, 100 test particles were tracked over

ISBN 978-3-95450-116-8

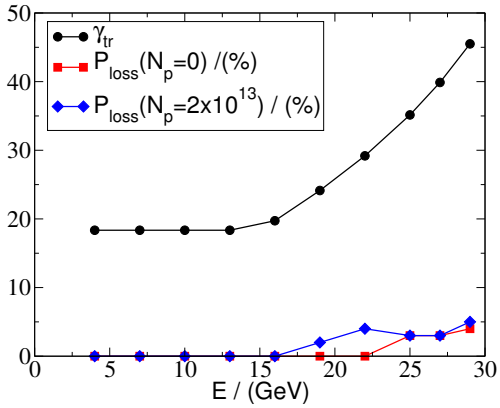

Figure 4: Beam loss without space charge and with space charge arising from 2×10^{23} protons as well as γ_{tr} as functions of the particle energy.

a period of of 16000 turns what is long enough to cover at least one synchrotron period for all energies considered The transverse initial coordinates of the test particles were chosen according to a bi-Gaussian distribution truncated at 2σ. The corresponding energy dependent rms emittances were $(\epsilon_{x,rms}, \epsilon_{y,rms})(E) = (3.25, 1)$ mm mrad $\beta_{in}\gamma_{in}/(\beta_E\gamma_E)$, where β_{in}, γ_{in} are the relativistic factors at injection energy and β_E, γ_E those of the energy considered. The momentum distribution was a Gaussian distribution truncated at two sigma with $\sigma = \delta_m/2$. According to the rf cycle of the proton ramp in SIS-100, the maximum momentum deviations were $\delta_m = 0.003$ at $E = 4$ GeV, $\delta_m = 0.005$ at $E = 7$ GeV, and $\delta_m = 0.004$ at $E = 29$ GeV [2]. Between 7 GeV and 29 GeV, δ_m was linearly interpolated. Beam loss up to 4 % was found, see red curve in in Fig. 4. Note, that these losses correspond to the sample of random magnet errors used in the simulations up to now. If choosing a different sample, the beam losses can change. In agreement with the γ_{tr} dependence of the dynamic aperture, also particle loss was found to occur only for high γ_{tr} or, more precisely, when $\gamma_{tr} > 25$ see the black curve in Fig. 4.

INCLUSION OF SPACE CHARGE

In this study only incoherent space charge effects were taken into account. The thin lens tracking tool of MAD-X was utilized to perform the simulations. Space charge could included only within the frozen space charge model. It was implemented by means of so called beambeam elements being elements implemented in MAD-X. They provide a transverse momentum kick according to a Gaussian beam shape truncated at two times the rms width. The rms width of each beambeam element was adapted to the rms width of the beam at its longitudinal position. Their implementation consists of two steps [3]. In the first step, marker elements are put at the positions of the beambeam kicks. Now the beta functions and, so the rms beam widths

$$z_{rms}(s) = \sqrt{\beta_z(s)\epsilon_{rms,z}} \text{ with } z = x, y \qquad (6)$$

can be determined. In the second step, the markers become replaced with the beambeam elements. In doing so, the oscillation of the space charge induced contribution to the betatron tune that arises from longitudinal particle motion through region of different space charge in the bunch was neglected.

Nevertheless, the results suggest the occurrence of space charge induced beam loss around $E = 20$ GeV, see blue curve in Fig. 4. The appearance of space charge induce beam loss below maximum energy seems reasonable because the influence of space charge is usually larger at lower energies. On the other hand, the appearance of a minimum energy is a hint for the necessity of complicated lattice functions arising from the high γ_{tr} optics for space charge induced beam loss to occur.

CONCLUSION

Aim of this paper was to present results from a tracking simulation study concerning the proton cycle in the SIS-100 synchrotron in order to do the first step in estimating beam loss. Key ingredient of the proton cycle is the usage of a high γ_{tr} lattice to keep the beam energy below the transition energy. This lattice causes lattice functions of strange shape. For that reason, the optics will be changed during the ramp in order to use the high γ_{tr} lattice only at high energies and to minimise the occurrence of difficulties due to the lattice functions. The tracking simulation were performed with MAD-X assuming constant energy. Effects due to synchrotron motion were regarded with respect to the tune change arising from the chromaticity. Space charge effects were included within the 2D frozen space charge model.

The results indicate that beam loss is generated by the complicated optics of the high γ_{tr} lattice. Space charge plays an important role at energies below the maximum energy. On the other hand, there is a lower energy limit for beam loss. That suggests that beam loss at medium energies is driven by the interconnection of space charge effects and the complicated high γ_{tr} optics.

Nevertheless, the present results are uncertain because the particle numbers in the simulation were small and only one sample of random errors was applied. Hence, the next step will be to repeat the simulations with larger particle numbers and for different random error samples to consolidate the results. Additionally, it would be desirable to perform simulations using codes which can model the influence of synchrotron motion on the space charge fields. These effects play a key role in the description of space charge induced beam loss in the presence of resonances.

REFERENCES

[1] V. Kapin and G. Franchetti, "The SIS100 Dipole and Quadrupole integrated kicks for nonlinear dynamics", GSI internal report ACC-note-2010-004, Darmstadt 2010.

[2] O. Chorniy, private communication.

[3] V. Kapin, private communication.

ISBN 978-3-95450-116-8